



Numerical modeling of industrial parts manufacturing using electromagnetic hemming process

Ilhem Boutana¹ · Abderrahmane Bousba² · Yaakoub Nadjari Benhadj²

Received: 20 January 2024 / Accepted: 23 May 2024 / Published online: 5 June 2024
© The Author(s), under exclusive licence to Springer-Verlag London Ltd., part of Springer Nature 2024

Abstract

In the contemporary times, *electromagnetic forming process* (EMF) is one of the most attractive high-velocity forming methods that can be used in order to achieve many industrial applications in sheet metal forming. Taking into account the advantages and limitations of EMF, this technology is highly used in the automotive industry and has increasing potential applications such as *Flanging*, *Bending*, and *Hemming* processes. Hemming is the process that bends the edges of sheets and serves to increase their stiffness and improve their appearance. In this paper, we aim to investigate *the simulation of forming Aluminum sheets using electromagnetic hemming process* in order to enhance our understanding of the process and its efficiency, particularly in industrial applications used for automotive panel production. Specifically, an electromagnetic bulging device serves as the fundamental setup for our various applications. This study undertakes multiple numerical simulations using the finite element method to explore the impact of process parameters on the deformed sheet. Additionally, we investigate the temperature distribution across the sheet during hemming. The numerical results demonstrate strong agreement with experimental data and existing research.

Keywords Electromagnetic forming · Sheet hemming · Finite element method · Deformation behavior

1 Introduction

Nowadays, high-velocity forming processes are stated to be the operations where the parts are requested at a high speed that exceeds 100 m/s. This kind of method includes other forming processes such as *explosive forming*, *electro-hydraulic forming*, and *electromagnetic forming* (EMF). All these methods can be differentiated from other forming methods [1]. They offer an acceleration of the part at high velocity via chemical, mechanical, or electrical forces. Furthermore, the kinetic energy of the pieces is significant [1, 2]. Among these process methods, electromagnetic forming has gained the focus of experts due to its economic issues and the fact that it has the advantage of increasing the production rate.

Aside from this, it is comfortable due to its high flexibility and repeatability. In addition, it allows a significant reduction in springback and improves the forming limitations that need to be addressed [3, 4].

Briefly, EMF depends on the magnetic induction effect. When a coil is placed near a conductor and pulsed via an energy store (i.e., a capacitor bank), a magnetic field is generated between this coil and the workpiece, providing the forming energy that accelerates the workpiece into die or drives it to a free-forming [1–4]. In fact, electromagnetic forming is an *impulse high-velocity forming technology* that uses high-voltage pulse current through an electromagnetic coil to generate a strong transient magnetic field that induces eddy currents in the nearby conductive workpiece. These eddy currents, in turn, produce an associated secondary magnetic field around the workpiece. This causes the coil and workpiece to repel each other by the electromagnetic force [1–3]. Based on the improved formability of EMF and its higher velocity, several studies have demonstrated electromagnetic process improvement (e.g., [4–6]). Depending on the arrangement of both the coil geometry and workpiece, different applications of electromagnetic forming can

✉ Ilhem Boutana
hafsaoui@univ-jijel.dz

¹ Laboratory of Electrical Engineering and Industrial Electronics, Faculty of Science and Technology, University of Jijel, Jijel 18000, Algeria

² Electrical Engineering Department, University of Jijel, Jijel 18000, Algeria

be achieved, such as compression and expansion of tubular components and many other sheet-forming applications such as *bulging, folding, welding, and hemming* (e.g., [1, 7]).

Moreover, hemming represents the process that bends the edge of a metal sheet to an angle of 180 degrees or more. It serves several functions, such as increasing the part stiffness, eliminating the acute edge, improving the appearance of highly visible panel edges, and joining the inner and outer parts. Hemming is usually applied as the last operation to be used in auto body panel production. Therefore, it has a crucial impact on the performance and quality of assembled vehicles. Flanging, bending, and hemming are the three steps of the sheet folding process that are used in the production of automotive closure panels [4, 8].

1.1 Motivations

Due to the required precision in the forming process and the complexity of the part, most of the bending, flanging, and hemming processes are tediously designed via lengthy and expensive die tests. EMF can be a good alternative solution for saving time, reducing costs, and improving the quality of hem joints, especially for Aluminum alloy applications (e.g., [7]).

Current initiatives in the automotive industry are driving a need for stronger and higher panels made of light materials, such as Aluminum parts. However, their lower formability creates considerable problems and issues [9, 10]. Furthermore, several studies have been performed in order to improve the quality of Aluminum parts (e.g., [1, 3]). In modern numerical manufacturing processes, simulation and modeling play an important role in the design and improvement of end-user parameters. For a long time, the modeling of electromagnetic forming faced different problems; however, along with the development and explosion of digital computing, it has become quite accessible. Several types of approaches can be performed and achieved (e.g., [11–13]). Semi-analytical methods can be used to solve simple problems, axially symmetric or planar, if the expression of the inductance is known [13]. Moreover, in general cases, the analytical expression for inductance is not known; it is then necessary to use numerical calculations, mainly the *finite element methods* (e.g., [14]).

Following these considerations, in this paper, we delve deep into the simulation of sheets forming through a magnetic hemming process, employing the power of finite element analysis harnessed through the *COMSOL MULTIPHYSICS software*. These calculations are performed in order to offer a better understanding of industrial processes using magnetic hemming, provide insights into the performance of the process, and investigate the formability and impact of process

parameters. This study pioneers the numerical simulation of the electromagnetic hemming process for many industrial applications of automotive parts, which is a pivotal advancement in the realm of industrial innovation. By unlocking the digitalization of automotive applications.

1.2 Paper organization

The remaining part of this paper is organized as follows. Section 2 focuses the attention on relevant related work to our research. In Sect. 3, we present the fundamental principle and the theoretical analysis of electromagnetic hemming. As well as introducing the mathematical models essential for achieving our numerical investigation. Section 4 discusses and describes our numerical models for each application, as well as the geometry and material properties. After that, in Sect. 5, we report our extensive applications and the results obtained. Finally, Sect. 6 provides conclusions and future work on our research.

2 State-of-the-art analysis

The process of electromagnetic hemming has garnered significant attention from researchers, leading to a wealth of publications that appeared in the active literature. This section aims to highlight some of the most pertinent and relevant works related to our research.

In [15], the authors propose a novel *joining procedure called hole-hemming*, specifically designed to unite *Magnesium AZ31* and *Aluminum AA6082-T4* alloy sheets to overcome the limited formability of Magnesium alloys at room temperature by adopting conventional joining techniques based on plastic deformation. Finite element analysis is employed to devise the joining process, identifying critical locations susceptible to fracture and analyzing their loading courses. The study further investigates the influence of process factors on the mechanical interlock to define appropriate process windows. In order to comprehensively evaluate the performance of the suggested hole-hemming process, they construct a flexible tool and experiment with diverse process parameters, achieving unique hole-hemmed joints for the first time. Subsequently, shear stress tests are conducted on single-lap joints to assess their strength and failure mechanisms. Overall, the study confirms the feasibility of hole-hemming as an effective approach to joining materials with significantly diverse formability, opening new possibilities for high-performance car construction in the automotive industry.

Conceição [16] presents a research effort focused on the development of a *flexible instrument tailored for the novel*

hole-hemming joining procedure, specifically for combining materials with significantly diverse mechanical characteristics. The study encompasses the design, fabrication, and assembly of various components constituting the hole-hemming tool, including structural, active, and passive elements, with a primary focus on achieving compatibility with dissimilar materials. The performance of the assembled tool is thoroughly assessed during experimentation, where the objective is to join an AA6082 – T4 Aluminum sheet (2 mm thick) with an AZ31 Magnesium sheet (0.9 mm thick). To validate the tool's effectiveness, experimental data is compared with the computational results obtained from finite element analysis of an ideal design.

In [17], the authors address the application of *hemming technology* in the automotive industry, specifically for joining inner and outer closure panels such as hoods, doors, and tailgates. Hemming involves the plastic deformation of the flange of the outer panel to fold it over the inner one, facilitating a secure and aesthetically pleasing connection. To ensure the successful final design of the part and equipment, a common feasibility study is essential. By categorizing and optimizing the feasibility study actions, the research aims to reduce equipment investment, minimize trial and error, achieve high-quality products, optimize cycle time, and expedite the commissioning period. The study relies on the results and challenges faced at each step, with a focus on identifying the root causes of errors or problems. This iterative approach allows for a comprehensive review and optimization of each aspect, leading to efficient and effective hemming processes in the automotive industry.

In [18], they focus their attention on investigating the *bending phenomena* of outer panels during the flanging, pre-hemming, and hemming processes, particularly in the context of automotive door panels and other types of panels. To achieve this, the researchers conducted an experimental study using a planar straight-edge-shaped hot-dip galvanized steel sheet panel. The study encompasses the flanging process to 90 degrees, followed by pre-hemming at 15 degrees, and finally, the hemming process. Throughout the experimental process, load profiles are recorded concerning the punch movement distance, and time-lapse images from videos of the processes are analyzed to examine changes in the panel's shape. Additionally, the researchers measured the *Micro Vickers hardness distribution* and obtained scanning electron microscope images of the panel's lateral surface. Notably, the study reveals new findings wherein both the microhardness and morphology of the panel change significantly during the flanging, pre-hemming, and hemming processes. These findings shed light on the intricate mechanisms involved in the bending and shaping of automotive door panels and other similar components.

In [19], the authors provide a comprehensive review of the latest advancements in high-speed forming conducted at the *Centre for Material Forming (CEMEF)*. The paper delves into the modeling strategy adopted for the simulation package, showcasing some noteworthy results for a ring expansion case. Moreover, they present the experimental settings implemented for the direct free-forming of flat metal sheets, aiming to complement the simulation findings with real-world observations. Overall, this work demonstrates a comprehensive and multi-faceted approach to exploring high-speed forming technologies through sophisticated simulations and practical experimentation. By combining advanced modeling techniques with real-world testing, the researchers at CEMEF contribute to the growing body of knowledge in the field of high-speed forming, opening up new possibilities for innovative manufacturing processes and materials engineering.

Other relevant related works in the field of electromagnetic forming processes can be found in [20–30].

3 Theoretical analysis of electromagnetic hemming process

In electromagnetic forming processes, a special tool coil is placed near the metal sheet, and an intense transient magnetic field, which is achieved by a pulse current generator, is employed to form electrically conductive materials. A typical EMF system consists of a bank of capacitors, a workpiece, and a coil. The energy stored in the capacitor bank is discharged through the coil in an alternative, damped electric current.

After the generation of a magnetic field, an eddy current is induced in the workpiece, which establishes another magnetic field around it. This secondary magnetic field, in turn, interacts with the original magnetic field, giving rise to a phenomenon known as electromagnetic repulsion. The mutually repulsive electromagnetic pressure between the stationary coil and the metal workpiece leads to the generation of intense, localized stress within the material. This high-pressure interaction ultimately results in significant plastic deformation of the workpiece. This transformation leads to the reshaping of the workpiece in response to the magnetic field's compelling directives.

EMF is fundamentally an *electro-thermo-mechanical process*. Different coupling strategies have been proposed to numerically solve this multiphysics problem. The strong coupling consists of solving the full set of equations at every step. This approach is the most accurate, but it leads to large non-symmetric matrices, which are computationally expensive in terms of solving time. Moreover, the EMF research progresses mainly via a combination of simulation

and experiments. However, with some experimentally complex equipment, the expert often needs to rely on simulations in order to investigate feasibility studies. Therefore, numerical models are highly necessary for this process (e.g., [31]).

Furthermore, these numerical models are needed to solve transient electrical circuits, electromagnetic equations, and the mechanical and thermal problems of the EMF process. Under a fully coupled model, including these different problems, the geometry displacement and forming speed of the workpiece will be comprehensively considered to further improve the calculation accuracy [32].

3.1 Electromagnetic theory

The forming system can be represented by an equivalent RLC circuit. The transient magnetic field analysis for an axially symmetric electromagnetic forming system is carried out based on the finite element method. The *magneto-dynamic equation* in terms of the magnetic vector potential, derived based on *Maxwell's equations*, is given by Eq. 1:

$$\sigma \frac{\delta A}{\delta t} + \text{curl} \left(\frac{1}{\mu} \cdot \text{curl} A \right) - \sigma \cdot \nu \cdot (\text{curl} A) = J_{ex} \quad (1)$$

where A is the magnetic vector potential, J denotes the current density in the coil, μ represents the magnetic permeability, and σ is the density.

From an electrical point of view, the forming coil and the workpiece have transformer coupling. The coil is the primary winding of the transformer, and the workpiece is considered a short-circuited secondary coil. By applying *Kirchhoff's laws*, the differential Eq. 2 is obtained:

$$\frac{d^2 I(t)}{dt^2} + 2\xi\omega \cdot \frac{dI(t)}{dt} + \omega^2 \cdot I(t) = 0 \quad (2)$$

such that $I(t)$ denotes the current caused by the discharging capacitor, ξ is the damping term given by: $\xi = (1/2) \cdot R \cdot (C/L)^{1/2}$, and ω represents the natural frequency given by: $\omega = (1/LC)^{1/2}$.

In EMF, ξ is less than one, which represents an under-damped system. Solving the above differential equation provides the current as a function of time. So the current flow through the circuit can be described by Eq. 3:

$$I(t) = V_0 \cdot \sqrt{\frac{C}{L}} \cdot \exp^{-\xi\omega t} \cdot \sin 2\pi f t \quad (3)$$

where V_0 is the original voltage across capacitor.

This time, the current signal in the coil produces a transient magnetic flux in the workpiece. The interaction between the two magnetic fields results in a material body force that

causes deformation of the workpiece. These body forces are commonly known as *Lorentz's forces*, which are expressed via Eq. 4:

$$F = J_e * B \quad (4)$$

where J_e and B represent eddy current density and magnetic flux density, respectively.

3.2 Structural mechanical theory

The workpiece is known to be plastically deformed in the EMF process. This can be described via *Newton's law* for the evaluation of deformation in the part in each time increment.

$$\rho \frac{\delta^2 u}{\delta t^2} - \nabla \cdot \sigma = F \quad (5)$$

where ρ is density, u represents the displacement vector, σ is the stress tensor, and F is the electromagnetic force density.

Since electromagnetic forming is a high-speed deformation process, a high *strain rate* impacts the mechanical properties of the workpiece. In this work, the *Johnson-Cook strength* model [33, 34] was adopted to characterize the stress flow for workpieces under a high strain rate. However, we used a simplified form of the *Johnson-Cook strength* model tailored for Aluminum [35, 36], as presented in Eq. 6:

$$\sigma = 93 \cdot (1 + 125 \cdot \varepsilon^{0.1}) \quad (6)$$

3.3 Thermal theory

Another phenomenon involved in electromagnetic forming is that it is governed by the equation of heat to get the temperature field in the time domain, which is given by Eq. 7:

$$\rho C_p \frac{dT}{dt} + \nabla \cdot (-k \cdot \nabla T) = Q \quad (7)$$

where k and ρC_p are the thermal conductivity and thermal storage capacity of the material, respectively.

Moreover, *Joule heating* is calculated in the workpiece material due to eddy current, and it is considered a heat source in thermal physics.

$$Q = \frac{1}{2} \cdot \sigma \cdot J_e^2 \quad (8)$$

4 Numerical modeling of electromagnetic hemming process

In this section, we discuss and describe our numerical models for each application (i.e., sheet bulging, bending, flanging,

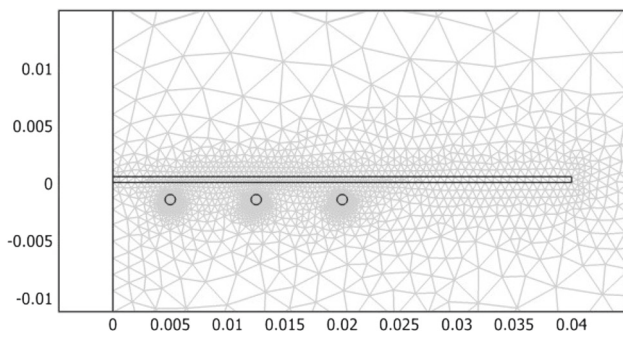


Fig. 1 Bulging device

and hemming), as well as presenting the geometry and material properties.

4.1 Sheet bulging system

In order to validate the above-described theoretical analysis, we start with a full analysis of the typical problem of forming flat parts in a sheet bulging system. This is considered the basis for other devices, which will be analyzed later.

The bulging device considered, which is presented in Fig. 1, is the same as the experimental installation [37], with a copper spiral coil under a thin Aluminum disc (radius of 0.04 m and thickness of 0.0005 m) fixed at its end. Table 1 presents all the system dimensions and parameters. Notably, due to the axial symmetry inherent in the geometry, the simulation in this model encapsulates only half of the system.

Table 1 System parameters

Parameter	Value
Number of coil turns	3, 5, 7
Coil conductivity (Copper)	5.998×10^7 [S/m]
Coil radius	20 [mm]
Workpiece radius	40 [mm]
Workpiece thickness	0.5 [mm]
Workpiece conductivity (Aluminum)	3.774×10^7 [S/m]
Resistance R	25.5 [mΩ]
Inductance L	2 [μH]
Capacity C	40 [μF]
Frequency f	17803 [Hz]
Voltage V_0	6470.52 [Volts]
Energy	0.84 [kJ]
Workpiece thermal conductivity	160 [W/(m * k)]
Density	2700 [kg/m ³]
Young's modulus	70×10^9
Poisson's ratio	0.33

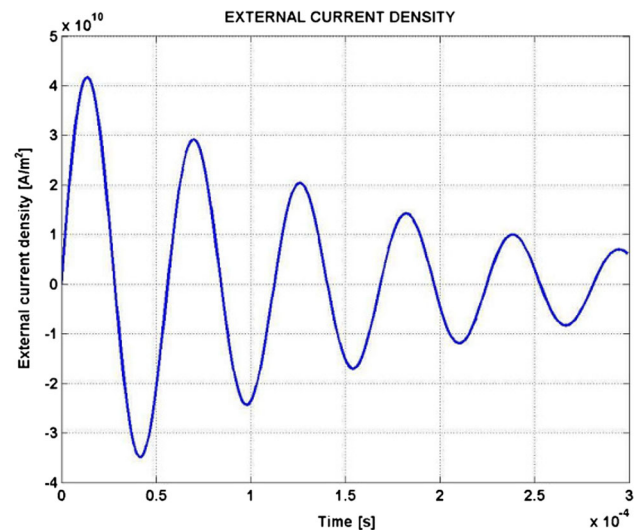


Fig. 2 External current density

Figure 2 illustrates the external current density employed within our simulation. This is derived from the discharge circuit, whose parameters are shown in Table 1. This waveform, given by Eq. 9, delineates the precise nature of the current employed in our computational model, which aligns meticulously with the experimental configuration to ensure congruence between simulated and real-world conditions (e.g., [37]).

$$J_0 = 4,556.10^{10} \cdot e^{-6372.8 \cdot t} \cdot \sin(1,12.10^5 \cdot t) \tag{9}$$

4.2 Bending model

The first step in hemming automotive panels consists of the bending operation. Under these specific conditions, the work-piece responds to the forces applied in a deliberate manner, yielding to the mechanical stress with an exactitude that yields a finely honed angle, where each facet of the bend is finely tuned to meet the exact requirements of the intended design or engineering specifications. The considered system is based on the previous bulging installation (see Fig. 1).

In order to guarantee and ensure the bending of the disc at this end, certain changes in the shape and dimensions of the coil become imperative. As a consequence, the number of turns was adjusted to 3, accompanied by a prescribed deflection width (fold width) of 11.5 mm, which is achieved by fixing the workpiece alongside another rigid disk boasting a radius of 28.5 mm, as shown in Fig. 3. This tailored configuration was instrumental in attaining the desired bending outcome in the disc, strategically adjusting the elements to achieve the intended experimental conditions.

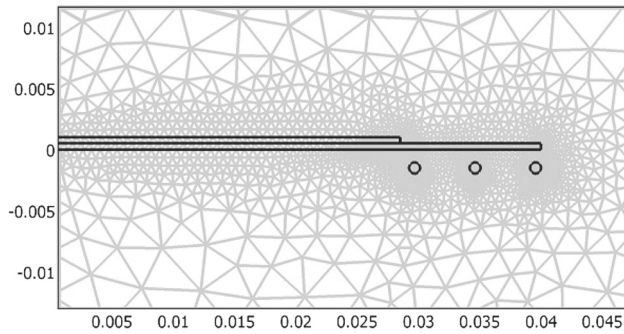


Fig. 3 Simulated bending system

4.3 Flanging models

Prior to performing the hemming operation, the parts need to be flanged. As shown in Fig. 4, to achieve the sheet hemming process, we keep the previous system by replacing the prior spiral coil with a tubular coil of 4 turns, which surrounds the disc. This tubular coil is located in front of the arrow part, with a width of 11.5 mm.

However, some industrial parts that are electromagnetically folded have concave or convex shapes. These specific forms were also performed by our numerical models using a tubular coil with 4 turns and a sheet bended at a 90-degree angle. This tubular coil is placed inside or outside of the sheet for convex or concave flanging, respectively. Figure 5 shows the flanging system for these specific forms.

4.4 Hemming model

In order to achieve a bend angle greater than 90 degrees, which is typically required for the sheet hemming process, a meticulous two-stage operation is performed. In the initial stage, we employ a tubular inductor with precisely 5 turns, strategically positioned in front of the upper edge of the bent piece at an exact 90-degree angle, as shown in Fig. 6.

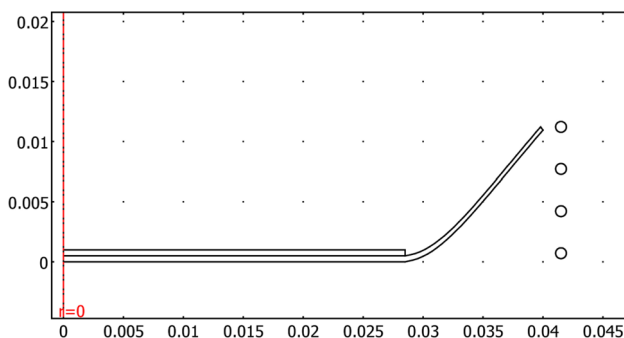


Fig. 4 Simulated sheet flanging system

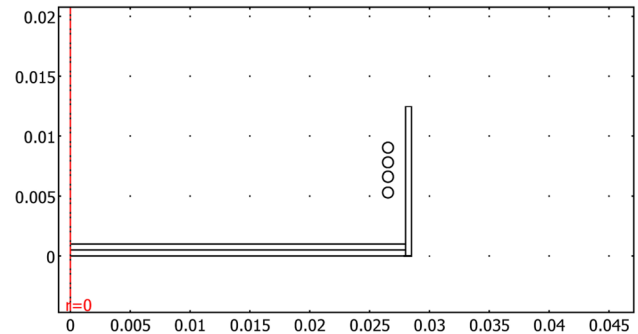


Fig. 5 Simulated sheet flanging system for concave and convex forms

For what concerns the second step, aimed at achieving the full hemming of the workpiece, an intricate and purpose-built coil configuration comes into play. This configuration is characterized by the incorporation of a complex-shaped coil, which comprises both a tubular coil with 3 turns and an additional flat coil, also consisting of 3 turns (see Fig. 7). This thoughtful configuration is critical in achieving a more accentuated and precise hemming of the workpiece, ensuring that the final result meets the exacting requirements of the manufacturing process.

Furthermore, an in-depth examination of the sheet material and its inherent characteristics (see Table 2) was conducted to meticulously scrutinize the variances in sheet behavior. This comprehensive study aimed to unravel the nuanced intricacies associated with the properties of the sheet and its dynamic nature.

5 Results and discussion

In this section, we delve deeper into the numerical simulations of electromagnetic hemming in industrial applications performed using the COMSOL MULTIPHYSICS software, which can fully couple electromagnetic, mechanical, and thermal systems. Our focus in this endeavor is mainly

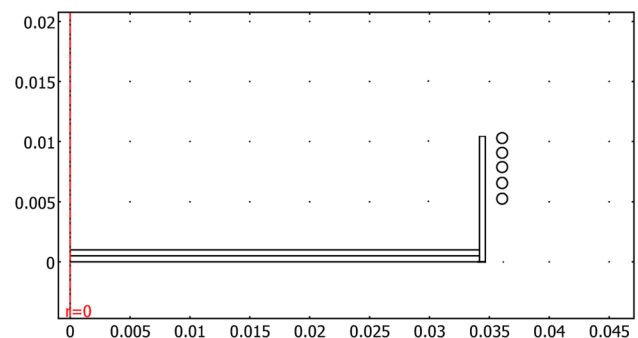


Fig. 6 Simulated first sheet hemming step system

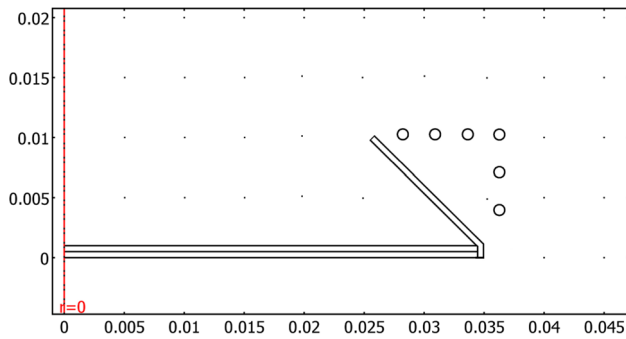


Fig. 7 Simulated second sheet hemming step system

oriented on innovative industrial processes, with a specific spotlight on the widely used magnetic bending and hemming techniques. These methods have revolutionized the way components are shaped and joined in the automotive manufacturing process, enhancing efficiency and precision to unprecedented levels.

Therefore, a transient analysis has been developed with a time step of $1 \mu s$. For each time step, the deformation and the temperature of the plate are evaluated, a new geometry is then created, and a new mesh is performed for a new time step calculation (see Sect. 4). The obtained numerical results are compared and validated by several experimental studies (e.g., [8, 38]).

5.1 Sheet bulging

The results of the numerical model presented in Fig. 8, show a plate deflection quite experimentally predicted by [1, 37, 39].

As illustrated in Fig. 8, the total deflection of the sheet (at $t = 300 \mu s$) is well-improved using inductors with a large number of turns. As a result, the sheet bulging is improved in the case of greater-radius coils. Moreover, when addressing the issue of heating in the formed part, it is essential to consider the theoretical insights presented in Fig. 9.

Table 2 Materials parameters

Parameter	Aluminum	Aluminum alloy 10150	Magnesium AZ31B
Electrical conductivity [s/m]	160	368	96
Thermal conductivity [W/(m*k)]	$3.774 e^7$	$3.448 e^7$	$1.087 e^7$
Young's modulus [Pa]	$70 \cdot 10^9$	$69 \cdot 10^9$	$45 \cdot 10^9$
Density [kg/m ³]	2700	2705	1770
Poisson's ratio	0.33	0.33	0.35

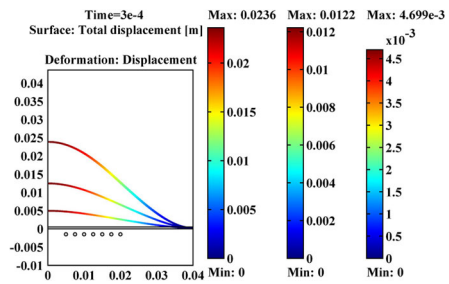


Fig. 8 Sheet bulging with 3, 5, and 7 turn coils

As shown in Fig. 9, it offers a clear visualization of the temperature distribution across the workpiece. Notably, the regions experiencing the highest temperatures correspond to those positioned directly opposite the turns of the coil. These specific areas are subject to the most intense eddy currents and magnetic forces generated during the process.

5.2 Bending process

In this work, a parametric analysis is carried out to analyze the effect of various bending setup parameters on the structural deformation of the bent disc (see Fig. 3). To study the impact of generator energy, we considered different current loads, which directly influence the magnetic, mechanical, and thermal behavior of the bent disc.

For the same forming time ($t = 300 \mu s$), the displacement (i.e., sheet bending) and temperature distribution for different generator energies are presented in Fig. 10a and b, respectively. These numerical results are theoretically confirmed by our numerical models.

On the other hand, considering different bending coils with different numbers of turns, we can conclude that this parameter has a significant effect but is lower than the generator power. Figure 10c and d show the effect of different bending coils on the sheet displacement and the temperature

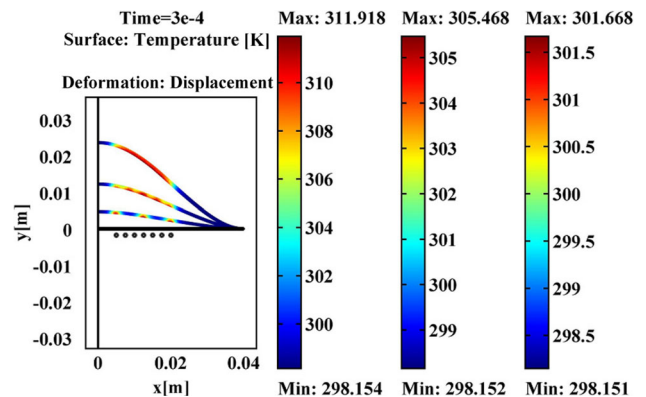


Fig. 9 Temperature distributions on bulged sheet

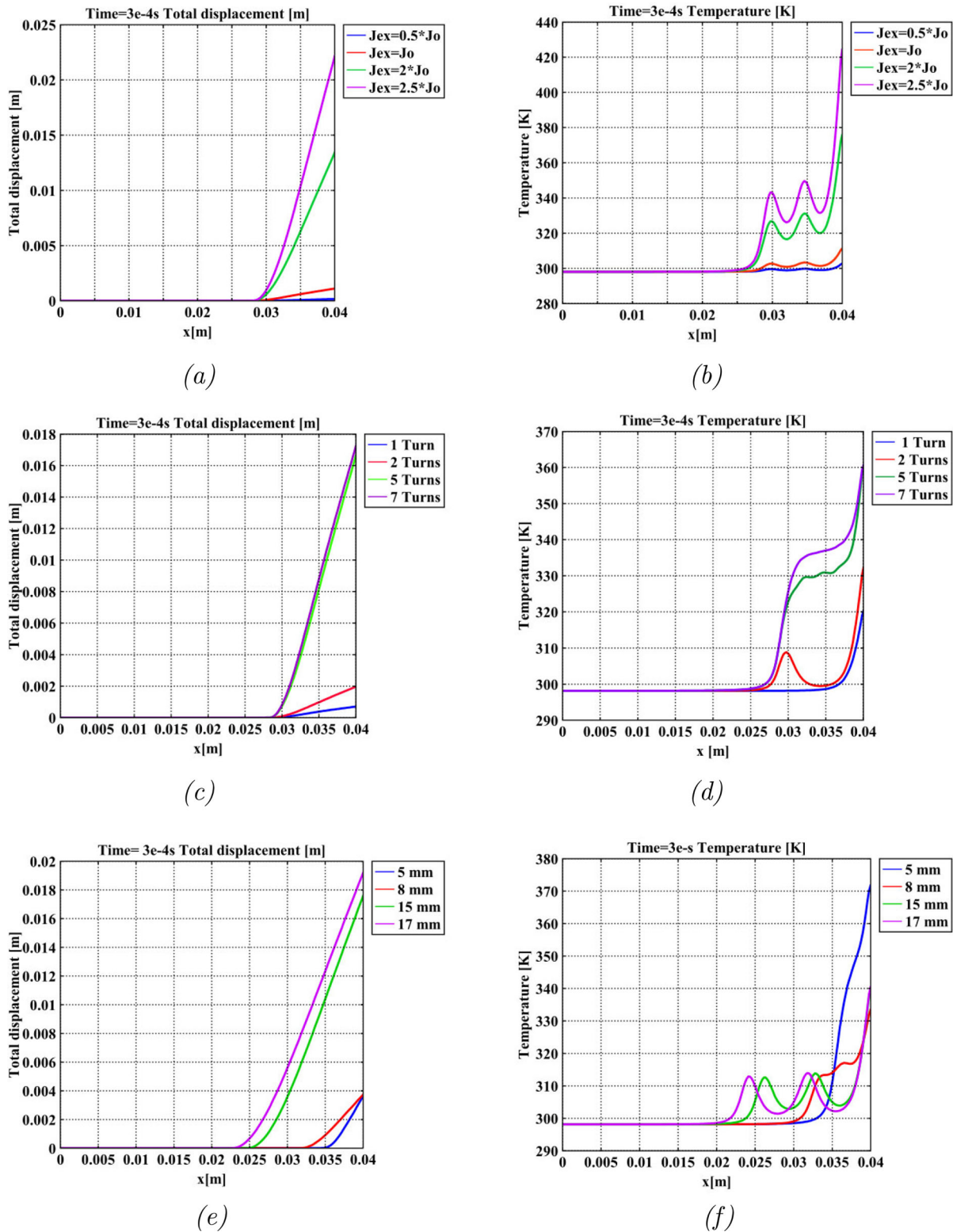


Fig. 10 Sheet bending for different generator energies (a), temperature distribution with different generators (b), sheet displacement with different coils (c), temperature distribution on a sheet bended with different

coils (d), sheet displacement with different fold width (e), temperature distribution on a sheet bended with different fold width (f)

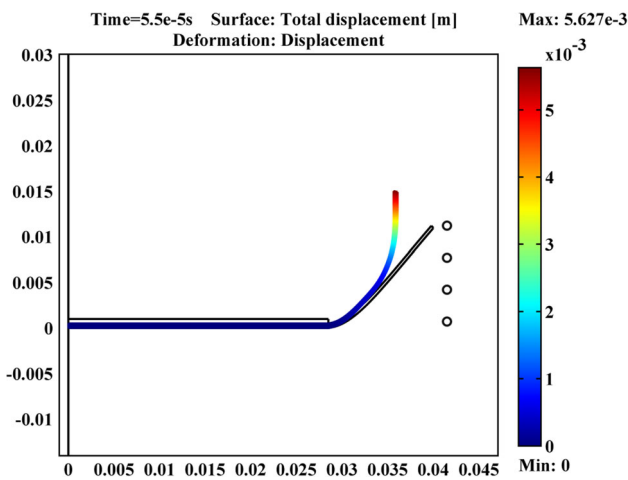


Fig. 11 Flanged sheet form

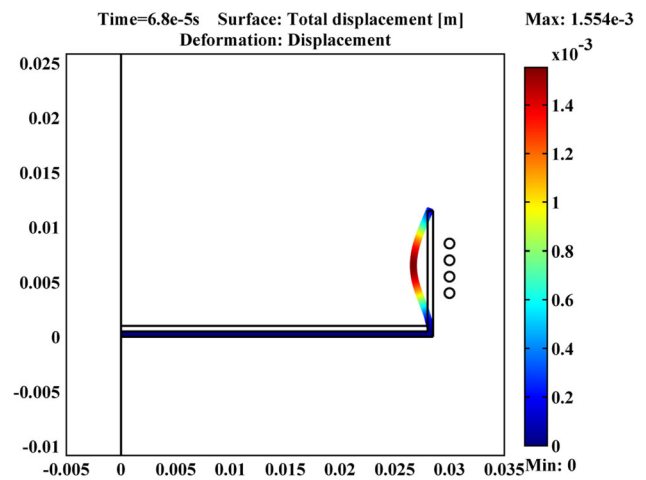


Fig. 13 Concave sheet flanging

distribution, respectively. In the following task, the number of coil turns is set to 3, and the power generator is about 1.26 KJ. Figure 10e presents the evaluation of the disc bending by varying the fold width, from 5 to 17 mm.

It is worth noting that the sheet deformation increases when the fold width is high and where the force is important. However, the temperature distribution stayed fixed and did not show high variation. Nevertheless, the maximum time of deflection is slightly affected, mainly by the number of coil turns, as displayed in Fig. 10.

5.3 Flanging process

Using the above geometrical system (see Fig. 4), the numerical model allows us to obtain a flanged sheet, as shown in Fig. 11.

Nevertheless, it is imperative to acknowledge that the simulated deformations do not manifest at the anticipated 90-

degree angle, with a radius of curvature equivalent to 7 mm, as depicted in Fig. 11. This deviation arises from a fundamental limitation in our numerical model, primarily centered around its axial symmetry.

Compounding this issue, the temperature profiles within the disc, as illustrated in Fig. 12. It is noteworthy that during the bending and bulging processes, the temperatures experienced by the sheet are notably higher than anticipated.

Furthermore, it is worth noting that certain automotive components designed for electromagnetic folding exhibit intricate concave or convex shapes, adding a layer of complexity to the manufacturing process. Notably, our numerical models have successfully captured and replicated these specific forms. These intricate shapes have been revealed by implementing a tubular coil with precisely 4 turns and bending a sheet at a precise 90-degree angle, as clearly demonstrated in Figs. 13 and 14.

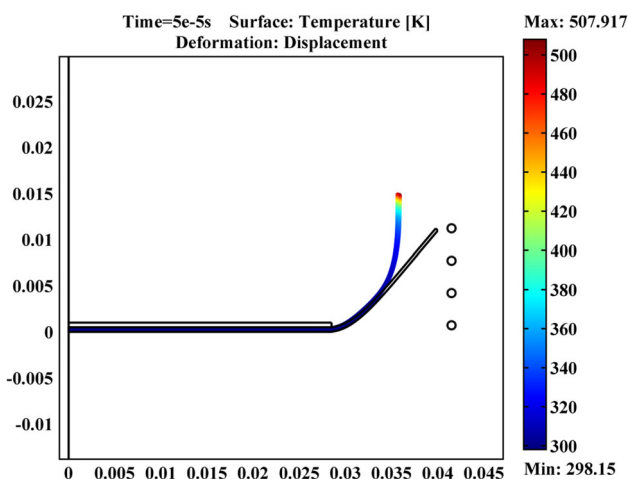


Fig. 12 Temperature distribution on flanged sheet

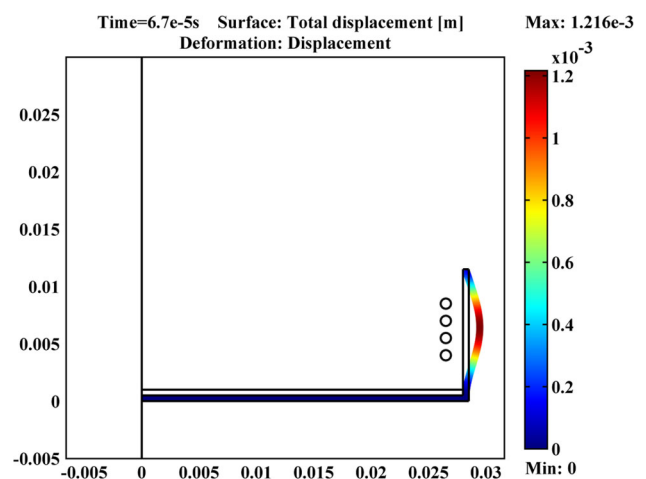


Fig. 14 Convex sheet flanging

This achievement underscores the versatility and predictive power of our numerical simulations in accurately replicating real-life manufacturing scenarios, which encompass a diverse range of complex automotive parts and their corresponding geometries.

The distinctive concave and convex flanging shapes are particularly accentuated as we push the boundaries with a higher number of coil turns and a surge in generator energy, which is vividly depicted in Fig. 15. This striking observation underscores the close relationship between these crucial process parameters and the ultimate shape achieved in the flanging process.

With an optimal number of coil turns and an energetic generator, the electromagnetic forces become more potent, effectively molding and contouring the material to create these highly accentuated, complex shapes in the flanged

automotive components. This finding further emphasizes the significance of optimizing these parameters to attain the desired curvature and geometry in the manufactured parts.

5.4 Hemming process

As presented in Sect. 4, our numerical model for the hemming process consists of a two-stage operation. The first phase, known as *pre-hemming*, initiates the deformation process and sets the foundation for what follows by creating a preliminary bend that serves as a crucial starting point for the subsequent stage, as presented in the numerical model shown in Fig. 6. Moreover, Fig. 16 shows the obtained shapes at different times for the first hemming step.

As displayed in Fig. 16, these visual representations offer valuable insights into the dynamic transformation of the

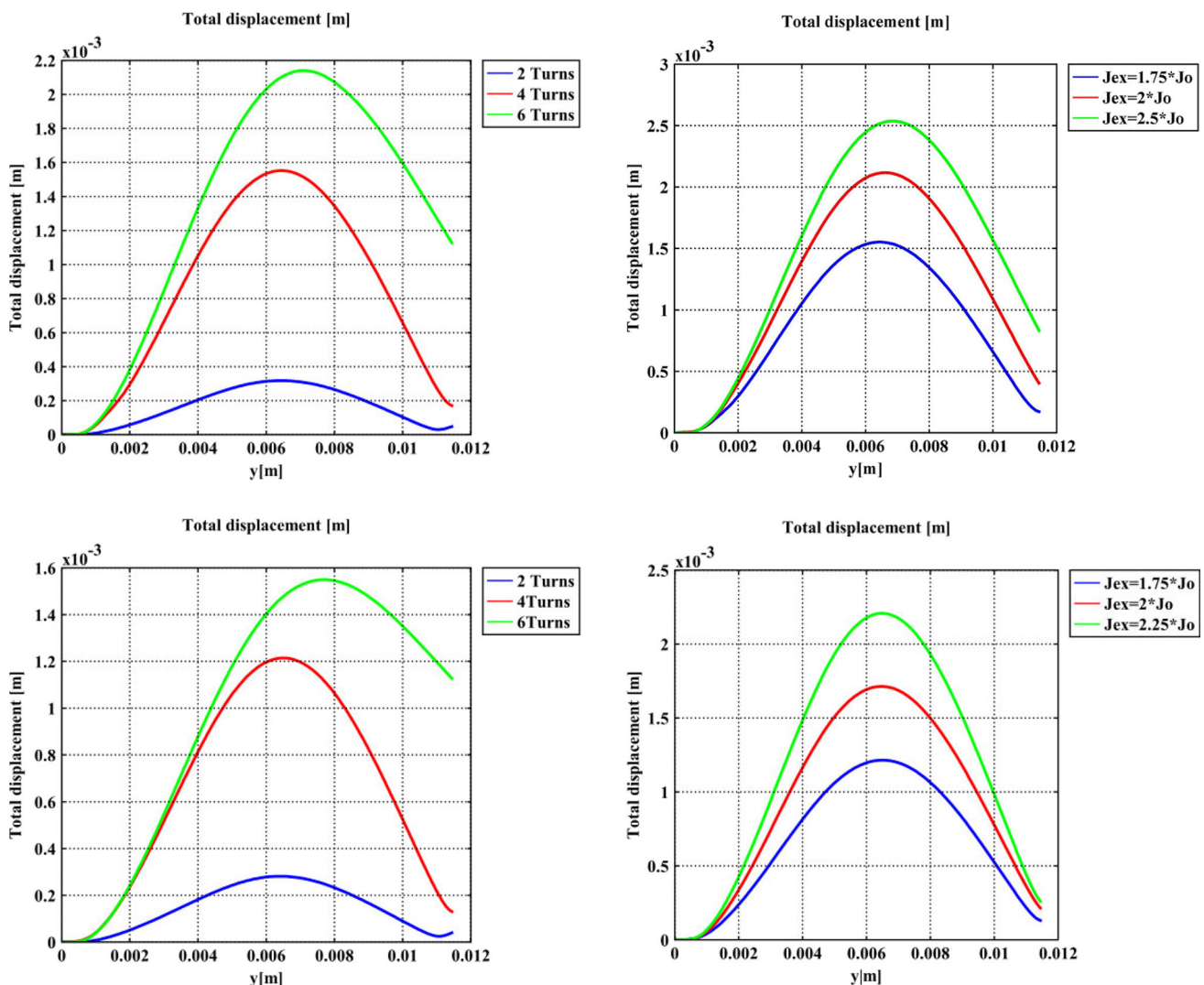


Fig. 15 Sheet concave flanging with different coils (a), sheet concave flanging with different generators (b), sheet convex flanging with different coils (c), sheet convex flanging with different generators (d)

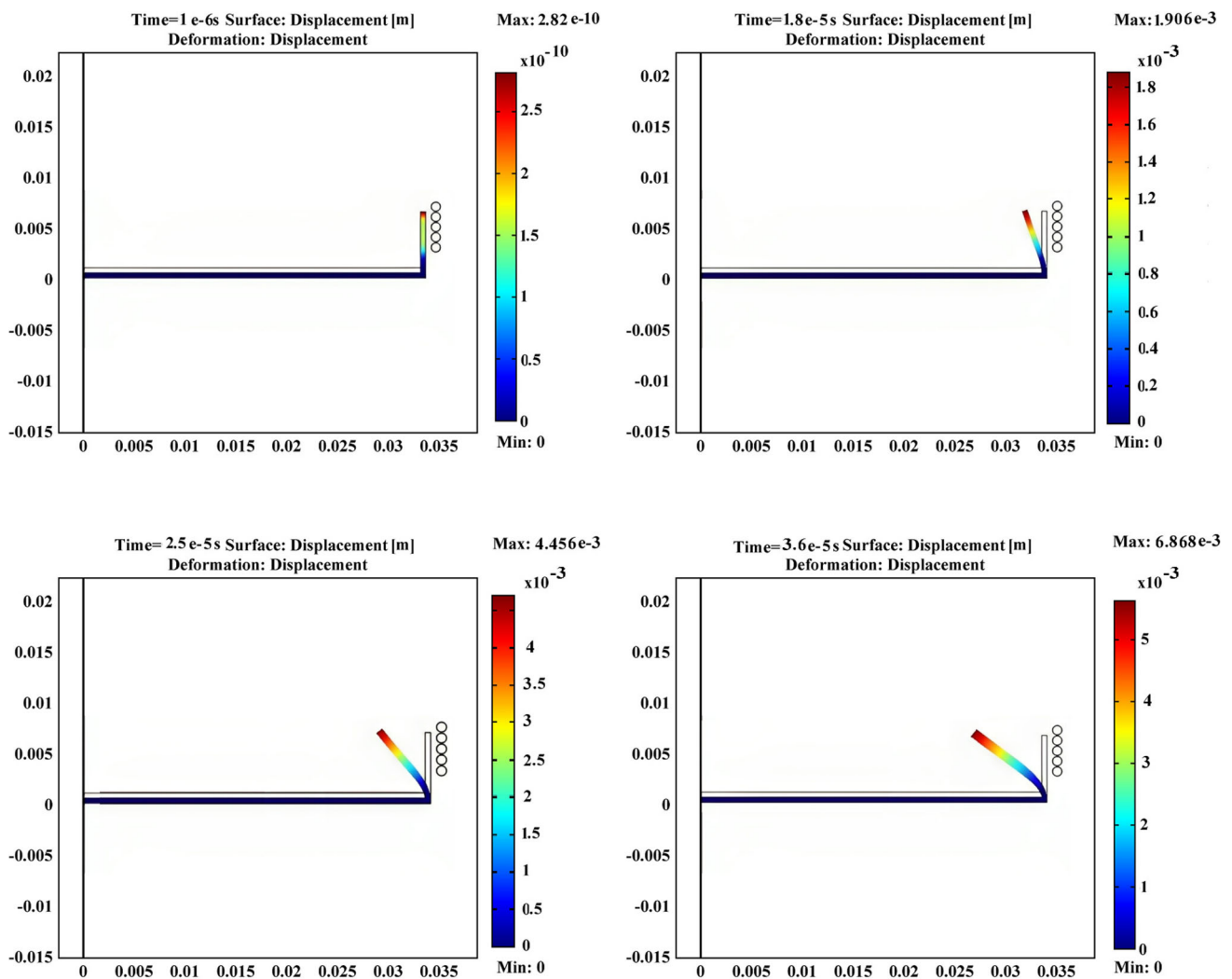


Fig. 16 The first sheet hemming step

material over time. It is evident that the results obtained, leveraging an energy input of 3.36 KJ , depict a folding of the workpiece by an angle of approximately 135 degrees after $36 \mu\text{s}$. Additionally, Fig. 17 shows the temperature distribution during this first hemming step. The ambient temperature exhibits a noticeable accentuation, with the most pronounced elevation occurring at the very tip.

By analyzing the results presented in Fig. 18, we can notice that Aluminum emerges as the material with the most favorable mechanical properties. This observation offers strong justification for the growing prevalence of Aluminum usage within the automotive industry [5, 9]. The exceptional mechanical performance of Aluminum and its alloys enhances their appeal in various automotive applications, ranging from structural components to lightweight materials, contributing to improved fuel efficiency and overall vehicle performance.

However, despite the increasing adoption of Magnesium in the industry, the numerical analysis brings to light a notable distinction. Unlike Aluminum, Magnesium does not exhibit superior mechanical behavior. In fact, it is revealed that Magnesium demands a higher energy input compared to Aluminum and its alloys to achieve comparable outcomes. This unique insight underscores the importance of selecting materials in the automotive sector, where considerations extend beyond mechanical properties alone.

To conclude, Magnesium popularity in the automotive realm primarily stems from its remarkably low weight, a highly sought-after attribute, particularly for economy cars. Therefore, while Aluminum excels in terms of mechanical performance, Magnesium's role in lightweight design remains significant, catering to the specific needs of the automotive market.

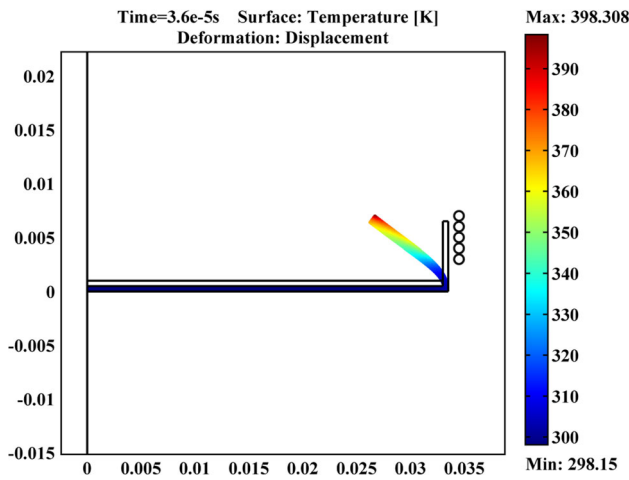


Fig. 17 Temperature distribution for the first sheet hemming step

Furthermore, in order to complete the hemming operation of the piece, we use the previously described geometrical configuration (see Fig. 7), allowing for a more acute folding of the component. In order to accommodate the heightened demands of this precise procedure, the generator used for discharge must have double the power. Figure 19 presents the sheet deformation results of the second hemming step.

As demonstrated in Fig. 19, the outcomes of this second sheet hemming step bear testimony to the effectiveness of this coil arrangement. The intricate and curvaceous contours showcased in the results underscore the precision and control

exercised in the hemming operation. This technique empowers the production process to realize the desired bend angles and geometries with a remarkable level of accuracy and precision.

The temperature distribution, thoughtfully presented in Fig. 20, provides a comprehensive perspective on the thermal effects induced during the process. Notably, the distribution reveals that despite the substantial heating involved, the material response remains well within acceptable and tolerable limits [6]. This critical observation underscores the robustness and resilience of the material in the face of elevated temperatures, assuring that it can withstand and adapt to the imposed thermal conditions without experiencing any adverse effects that might compromise its structural integrity or mechanical properties. This, in turn, reinforces the viability and safety of the manufacturing process, assuaging concerns related to potential material degradation due to temperature.

5.5 Discussion and remarks

In this section, we provide a discussion of our obtained results from different applications, as well as comparing them with some related research from the active literature.

First, for the bulging system that is considered the basis of all other systems used in the hemming processes, the obtained numerical results are compared with experiments conducted by [37, 39].

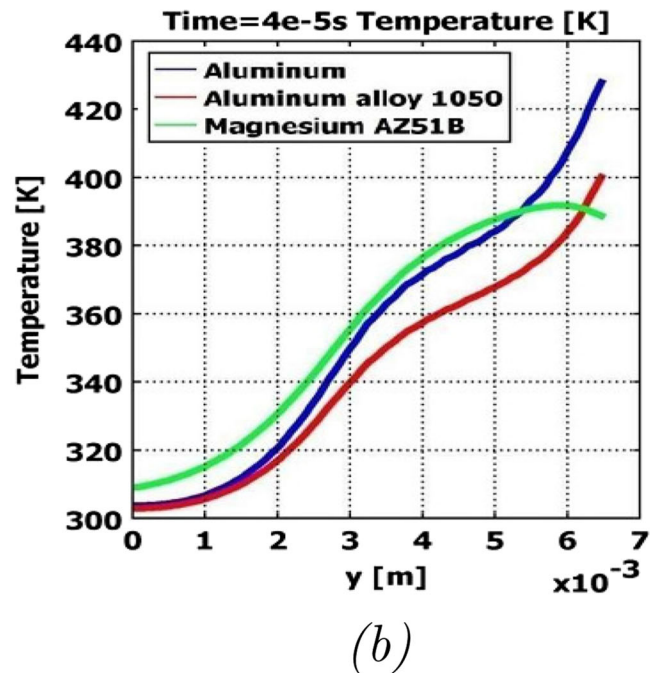
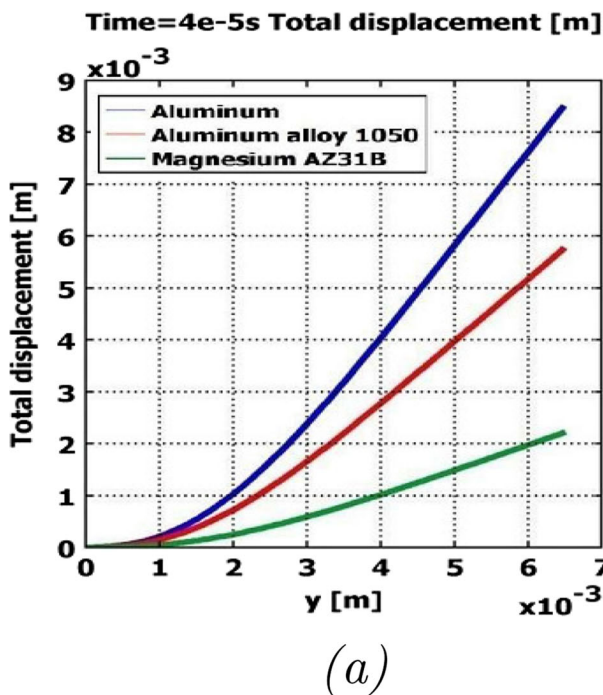


Fig. 18 Displacement of different folded sheets (a), temperature distributions for different sheets (b)

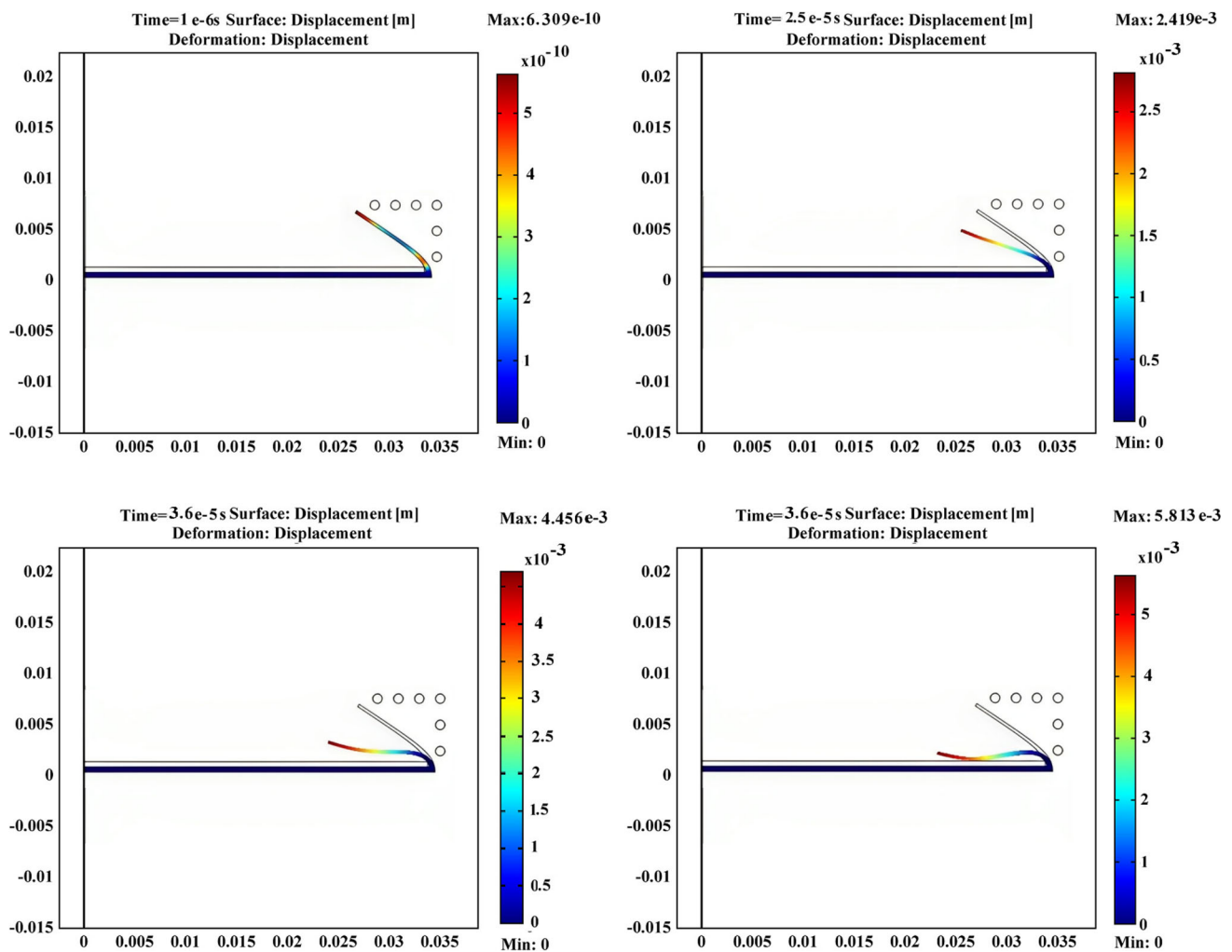


Fig. 19 The second sheet hemming step

Akbar et al. [39] developed a setup for *high-stain-rate electromagnetic forming of thin Aluminum sheets* by using a flat spiral coil and a capacitor bank of 4 kJ and 8.9 kJ. Indeed, they conducted sheet-forming experiments for different sheet thicknesses (0.5, 0.8, 1.0, 1.2, 1.5, and 2.0 mm), using a coil with 13 turns. However, in our case and as presented in Sect. 4, we used a copper spiral coil with 3, 5, and 7 turns under a thin Aluminum disc (radius of 0.04 m and thickness of 0.5 mm).

For what concerns the numerical results (see Sect. 5), the total deflection of the sheet seems to be improved using inductors with a large number of turns. As a result, the sheet bulging is improved in the case of greater-turn coils, which leads to the same conclusion as the experimental setup [39]. Table 3 summarizes the comparison between our numerical results and those of [37, 39].

As can be seen from Table 3, our numerical results are in good agreement with those of [37], since we consider a

similar bulging system comprising pancake coils with several turn windings and circular Aluminum workpieces.

In fact, Takatsu et al. [37] have developed an analytical model to predict the sheet deflection in free bulging cases. In addition, they confirmed their results by conducting experiments. They use a coil with five turns, but we use various coils with 3, 5, 7 turns to study the effect of the number of coil turns (the coil radius) on sheet deflection. However, the comparison with the numerical works of Akbar et al. [39], conducted using *FEMM software*, can be only qualitative, since the design of the coil was modified with 13 turns.

Moreover, for what concern the flanging process, Table 4 summarizes our numerical results by highlighting the effect of three factors: (i) the energy of the bending generator; (ii) the number of coil turns; (iii) the fold width on sheet bending and consequently on the flanging angle. This numerical result can be compared with those of [40].

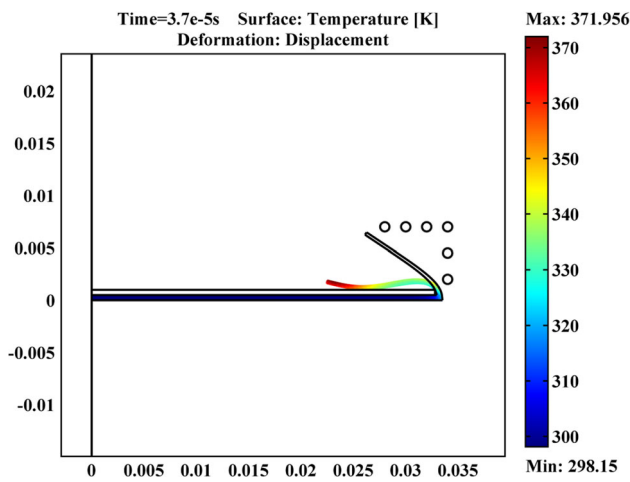


Fig. 20 Temperature distribution for the second sheet hemming step

Table 4 Comparison of flanging angle

Fold width [mm]	Generator energy [KJ]	Number of coil turns	Flanging angle [degree]
3	1.26	3	35
8	1.26	3	23.6
11.5	0.42	3	4.97
11.5	0.84	3	9.86
11.5	1.26	1	3.73
11.5	1.26	2	9.87
11.5	1.26	5	66
11.5	1.26	7	66
11.5	1.68	3	50.6
11.5	2.1	3	62.4
15	1.26	3	49.4
17	1.26	3	48.18

As shown in Table 4, as expected, the flanging angle increases significantly with increased coil radius. So, the number of coil turns has a significant effect on the bending angle. but fold width affects it less than the above parameter. In fact, energy input is the parameter that has the greatest effect on sheet bending and its angle.

However, Despite the fact that in [40], they used an experimental bending and flanging setup with a non-spiral coil that has a special shape, our results are well-confirmed by their flanging experiments. Specifically, we do not have the same input parameters for the flanging process, but the angles of flanging are within the same range.

Finally, as regards the hemming process, we qualitatively compared our results with the experimental ones. Jimbert et al. [7], Anderson et al. [25] have conducted a characterization of electromagnetic hemming using several parameters, namely the *outer diameter*, the *overlapping between coil and flange* and the *roll-in parameter* that quantifies the flanging quality. However, it would be interesting to study the variation of these parameters over each other.

As presented in Sect. 4, and although in our modeling process we have adopted a two-stage process (similarly to conventional hemming), which is different from the experimental setup [7, 25], the numerical results obtained highlight the efficiency of this electromagnetic hemming process (see Sect. 5). The outcomes of the sheet hemming process attest to the effectiveness of our coil arrangement (a tubular inductor with precisely 5 turns in the first step, while in the second step, we incorporated a complex-shaped coil, which comprises both a tubular coil with 3 turns and an additional flat coil, also consisting of 3 turns) in realizing the desired bend angles and geometries with a remarkable level of accuracy and precision. Indeed, Table 5 highlights the comparison between our hemming results and those of [7, 25].

Therefore, our numerical results presented in Table 5 align well with those obtained experimentally by [7, 25], given the different materials of the considered parts (resulting in different mechanical parameters of the parts) as well as the geometry and dimensions of the used inductors. Indeed, studying other output parameters (e.g., *union radius*, *warp*

Table 3 Comparison of depth sheet bulging

	Model	Geometry		Deflection time [μ s]	Number of coil turns	Max sheet displacement [mm]	Max sheet temperature [K]
		Sheet radius [mm]	Sheet thickness [mm]				
Our Model	COMSOL Software	40	0.5	300	3	4.7	301.5
			5		12.2	305.468	
			7		23.6	311.918	
[37]	Experiments	40	0.5	215	5	20	/
	Analytical model	40	0.5	211.7 – 269.3	5	17	/
[39]	FEMM Software	32	6.75	/	13	25 – 28	/

Table 5 Comparison between hemming parameters

	Specification	Fold width [mm]	Outer diameter [mm]	Overlap [mm]	Roll-in [mm]
Our model	Spiral coils	11.5	35	> 8	< 0.5
[25]	Circular coils	20	30	> 40%	0.8
[7]	Circular coils	5 – 7	120	15% – 60%	3

defects) would be desirable. Additionally, the geometrical shape and dimensions of the hemming coil can also be improved in further investigations.

In summary, the numerical results we have presented find solid validation and affirmation in the extensive body of active literature on this subject (e.g., [8, 25, 41]). Within the current landscape of research and practical applications, there exists a wealth of experimental evidence that aligns closely with the outcomes of our numerical analysis (e.g., [1, 25, 37, 39]). This convergence between our computational results and empirical data underscores the reliability and accuracy of our models, reinforcing our confidence in their ability to mirror real-life scenarios with a high-degree of efficiency.

6 Conclusions and future work

In this paper, the purpose was to develop numerical models in order to study and simulate many EMF industrial devices. This study presents a simulation of an innovative approach to hem metal sheets by electromagnetic forming, using several coils with different forms. It proves the feasibility of EMF for flanging, bending, and hemming operations in industrial parts. By making the process very suitable for the production of specific applications at high production rates, particularly in the automotive industry. These finite element simulations were carried out to investigate the formability and deformation behavior under the hemming process. These models have allowed us to preview the electromagnetic forces that workpieces are subject to and consequently allowed us to calculate deflections and temperature in different time steps during the electromagnetic hemming processes.

This numerical study, although validated by experimental results, does not remain without limits. Because they are two-dimensional with axial symmetry, they cannot simulate all the industrial applications; three-dimensional models are necessary and will be our next investigations. Another aspect of future works is mainly oriented toward emerging *electromagnetic trends* (e.g., [42–46]).

Author contribution I. Boutana: conceptualization, formal analysis, methodology, supervision, validation, resources, writing — original draft, writing — review and editing; A. Bousba: methodology, validation, resources, writing — original draft; Y. Nadjari Benhadj: method-

ology, validation, resources, writing — original draft. All authors have reviewed the manuscript.

Declarations

Conflict of interest The authors declare no competing interests.

References

- Kamal M, Daehn GS (2006) A uniform pressure electromagnetic actuator for forming flat sheets. *J Manuf Sci Eng* 129(2):369–379. <https://doi.org/10.1115/1.2515481>
- Dehra MS (2006) High velocity formability and factors affecting it. PhD thesis, The Ohio State University
- Motoasca MT (2003) Electrodynamics in deformable solids for electromagnetic forming. PhD thesis, Transylvania University
- Reddy BL, Rao BC, Reddy PR, Reddy PVRR (2014) A review on springback in metal forming. *Int J Eng Res Technol* 3(1):646–655
- Miller WS, Zhuang L, Bottema J, Wittebrood AJ, De Smet P, Haszler A, Vieregge A (2000) Recent development in aluminium alloys for the automotive industry. *Mater Sci Eng: A* 280(1):37–49. [https://doi.org/10.1016/S0921-5093\(99\)00653-X](https://doi.org/10.1016/S0921-5093(99)00653-X)
- Chunfeng L, Zhiheng Z, Jianhui L, Yongzhi W, Yuying Y (2002) Numerical simulation of the magnetic pressure in tube electromagnetic bulging. *J Mater Process Technol* 123(2):225–228. [https://doi.org/10.1016/S0924-0136\(02\)00063-8](https://doi.org/10.1016/S0924-0136(02)00063-8)
- Anderson R, Brännström P, Daehn G, Eguia I, Gonzalez B, Gutierrez M, Jimbert P, Olsson S, Sundberg H, Zhang Y (2008) Flanging and hemming of auto body panels using the electro magnetic forming technology. In: 3rd International conference on high speed forming, March 11–12, 2008, Dortmund, Germany. <https://doi.org/10.17877/DE290R-14136>
- Golovashchenko SF (2005) Sharp flanging and flat hemming of aluminum exterior body panels. *J Mater Eng Perform* 14:508–515. <https://doi.org/10.1361/105994905X56142>
- Krajewski PE, Carsley JE (2003) Heat treatment effects on bending in aa6111. TMS Annual Meeting, pp 25–32
- Kumar R, Kore SD (2019) Effect of the field shaper geometries in electromagnetic crimping of tubes on rods. *J Manuf Sci Eng* 141(11):114501. <https://doi.org/10.1115/1.4044516>
- Boutana I, Mekideche MR, Bali H (2023) Analysis model and numerical investigation of electromagnetic tube expansion with field concentrator. In: 2023 20th International multi-conference on systems, signals & devices (SSD), pp 294–298. <https://doi.org/10.1109/SSD58187.2023.10411205>. IEEE
- Boutana I, Bouferroum SE, Laouira A (2022) Modeling of the innovative magnetic pulse joining technology. In: 19th International multi-conference on systems, signals & devices (SSD), Setif, Algeria, pp 2115–2120. <https://doi.org/10.1109/SSD54932.2022.9955979>

13. Thomas JD, Triantafyllidis N (2009) On electromagnetic forming processes in finitely strained solids: theory and examples. *J Mech Phys Solids* 57(8):1391–1416. <https://doi.org/10.1016/j.jmps.2009.04.004>
14. Safa S (2023) Feasibility study of the robot-roller hemming process. PhD thesis, Bursa Uludag University
15. Pereira JAC, Kasaei MM, Carbas RJC, Marques EAS, Lim H, da Silva LFM (2023) Joining magnesium and aluminum alloy sheets by a novel hole hemming process. *Thin-Walled Struct* 187:110758. <https://doi.org/10.1016/j.tws.2023.110758>
16. Conceição AGC, Kasaei MM, Carbas RJC, Marques EAS, Silva LFM (2023) A flexible tool for joining dissimilar materials by the novel hole hemming process. *Mechanics based design of structures and machines*, pp 1–29. <https://doi.org/10.1080/15397734.2023.2197041>
17. Kasaei MM, Silva LFM (2022) Joining sheets made from dissimilar materials by hole hemming. *Proc Inst Mech Eng Part L: J Mater: Des Appl* 236(6):1321–1332. <https://doi.org/10.1177/14644207211072676>
18. Takatsu S-I, Aoki Y, Nitta Y, Komoto T, Kumehara H, Lin W (2022) Experimental study on strain hardening of steel panels in the hemming process. *Adv Mater Process Technol* 8(2):2069–2086. <https://doi.org/10.1080/2374068X.2021.1878731>
19. Alves JR, Bay F (2015) Magnetic pulse forming: simulation and experiments for high-speed forming processes. *Adv Mater Process Technol* 1(3–4):560–576. <https://doi.org/10.1080/2374068X.2015.1132723>
20. Cui X, Li S, Feng H, Li G (2017) A triangular prism solid and shell interactive mapping element for electromagnetic sheet metal forming process. *J Comput Phys* 336:192–211. <https://doi.org/10.1016/j.jcp.2017.02.014>
21. Cui X-H, Mo J-H, Zhu Y (2012) 3d modeling and deformation analysis for electromagnetic sheet forming process. *Trans Nonferr Metal Soc China* 22(1):164–169. [https://doi.org/10.1016/S1003-6326\(11\)61156-4](https://doi.org/10.1016/S1003-6326(11)61156-4)
22. Psyk V, Risch D, Kinsey BL, Tekkaya AE, Kleiner M (2011) Electromagnetic forming—a review. *J Mater Process Technol* 211(5):787–829. <https://doi.org/10.1016/j.jmatprotec.2010.12.012>
23. Walkea GA, Kulkarni A, Vasudevana R (2014) Finite element analysis and parametric study of electromagnetic forming process. *Int J Eng Res Technol* 3(12)
24. Bali H, Hafsaoui I, Makhlouf B (2018) A simultaneous resolution method for coupling field_circuit equations for steady-state skin effect problems. In: 2018 International conference on electrical sciences and technologies in Maghreb (CISTEM), Algiers, Algeria, pp 1–6. <https://doi.org/10.1109/CISTEM.2018.8613543>
25. Jimbert P, Eguia I, Perez I, Gutierrez MA, Hurtado I (2011) Analysis and comparative study of factors affecting quality in the hemming of 6016t4aa performed by means of electromagnetic forming and process characterization. *J Mater Process Technol* 211(5):916–924. <https://doi.org/10.1016/j.jmatprotec.2010.08.022>
26. Boutana I, Mekideche MR (2009) Finite element model analyzing dynamical behavior of sheet electromagnetic forming. In: 6th International multi-conference on systems, signals and devices (SSD), Djerba, Tunisia, pp 1–6. <https://doi.org/10.1109/SSD.2009.4956684>
27. Qiu L, Zhang W, Abu-Siada A, Xiong Q, Wang C, Xiao Y, Wang B, Li Y, Jiang J, Cao Q (2020) Electromagnetic force distribution and wall thickness reduction of three-coil electromagnetic tube bulging with axial compression. *IEEE Access* 8:21665–21675. <https://doi.org/10.1109/ACCESS.2020.2969678>
28. Boutana I, Mekideche MR (2008) Simulation of aluminum sheet electromagnetic forming with several dies. In: 2008 5th International multi-conference on systems, signals and devices (SSD), Amman, Jordan, pp 1–6. <https://doi.org/10.1109/SSD.2008.4632852>
29. Huang L, Zhang J, Zou J, Zhou Y, Qiu L (2019) Effect of equivalent radius of drive coil on forming depth in electromagnetic sheet free bulging. *Int J Appl Electromagn Mech* 61(3):377–389. <https://doi.org/10.3233/JAE-190009>
30. Yu G, Guo D, Zou S (2022) Production capacity improvement of hood production line based on the theory of constraints. In: 2022 8th International conference on mechanical engineering and automation science (ICMEAS), Wuhan, China, pp 111–116. <https://doi.org/10.1109/ICMEAS57305.2022.00029>
31. Boutana I, Bahloul A, Boukendir S (2021) Numerical investigation on weldability of workpieces using magnetic pulse welding process. In: 2021 IEEE international conference on design & test of integrated micro & nano-systems (DTS), Sfax, Tunisia, pp 1–6. <https://doi.org/10.1109/DTS52014.2021.9498108>
32. Qiu L, Zhang W, Abu-Siada A, Liu G, Wang C, Wang Y, Wang B, Li Y, Yu Y (2020) Analysis of electromagnetic force and formability of tube electromagnetic bulging based on convex coil. *IEEE Access* 8:33215–33222. <https://doi.org/10.1109/ACCESS.2020.2974758>
33. Khan Z, Khan M, Jaffery SHI, Younas M, Afaq KS, Khan MA (2020) Numerical and experimental investigation of the effect of process parameters on sheet deformation during the electromagnetic forming of aa6061-t6 alloy. *Mech Sci* 11(2):329–347. <https://doi.org/10.5194/ms-11-329-2020>
34. Johnson GR, Cook WH (1983) A constitutive model and data for materials subjected to large strains, high strain rates, and high temperatures. In: 7th International symposium on ballistics, pp 541–547
35. Patil SP, Prajapati KG, Jenkouk V, Olivier H, Markert B (2017) Experimental and numerical studies of sheet metal forming with damage using gas detonation process. *Metals* 7(12). <https://doi.org/10.3390/met7120556>
36. Deng H, Mao Y, Li G, Cui J (2019) A study of electromagnetic free forming in aa5052 using digital image correlation method and fe analysis. *J Manuf Process* 37:595–605. <https://doi.org/10.1016/j.jmapro.2018.12.033>
37. Takatsu N, Kato M, Sato K, Tobe T (1988) High-speed forming of metal sheets by electromagnetic force. *JSME Int J Ser 3 Vibr Control Eng Ind* 31(1):142–148
38. Shang J, Wilkerson L, Hatkevich S (2011) Hemming of aluminum alloy sheets using electromagnetic forming. *J Mater Eng Perform* 20:1370–1377. <https://doi.org/10.1007/s11665-011-9988-y>
39. Akbar S, Aleem MA, Sarwar MN, Zillohu AU, Awan MS, Haider A, Ahmad Z, Akhtar S, Farooque M (2016) Electromagnetic flat sheet forming by spiral type actuator coil. *IOP Conf Ser: Mater Sci Eng* 146(1):12054. <https://doi.org/10.1088/1757-899X/146/1/012054>
40. VanBenthysen R, Kinsey B (2010) Microflanging of cuzn30 specimens using electromagnetic forming. *HIGH SPEED FORMING* 2010:208
41. Lai Z, Cao Q, Chen M, Liu N, Li X, Huang Y, Han X, Li L (2019) The effect of coil polarity on electromagnetic forming using a multi-coil system. *Int J Adv Manuf Technol* 103:1555–1566. <https://doi.org/10.1007/s00170-019-03656-8>
42. Boutana I, Boussalem ME, Laouira A, Bouferrou S (2022) 3d modelling of the mechanical behaviour of magnetic forming systems. *Bull Electr Eng Inform* 11(4):1807–1817. <https://doi.org/10.11591/eei.v11i4.3628>
43. Xiong Q, Tang H, Wang M, Huang H, Qiu L, Yu K, Chen Q (2019) Design and implementation of tube bulging by an attractive electromagnetic force. *J Mater Process Technol* 273:116240. <https://doi.org/10.1016/j.jmatprotec.2019.05.021>
44. Satonkar N, Gopalan V (2023) Simulation of electromagnetic forming process and optimization of geometric parameters of per-

- forated al sheet using rsm. *Mathematics* 11(9). <https://doi.org/10.3390/math11091983>
45. Ye X, Yang C, He E, Yang P, Gao Q, Yan T, Yin S, Ye Y, Wu H (2023) Electromagnetic wave absorption properties of the fesial/pla and fesial-mos2-graphene/pla double-layer absorber formed by fused deposition modeling. *J Magn Magn Mater* 565:170280. <https://doi.org/10.1016/j.jmmm.2022.170280>
46. Thirupathi N, Kumar R, Kore SD (2023) Non-coupled finite element modelling of electromagnetic radial compaction of pure aluminium powder. *Int J Precis Eng Manuf* 24:325–336. <https://doi.org/10.1007/s12541-022-00750-y>

Publisher's Note Springer Nature remains neutral with regard to jurisdictional claims in published maps and institutional affiliations.

Springer Nature or its licensor (e.g. a society or other partner) holds exclusive rights to this article under a publishing agreement with the author(s) or other rightsholder(s); author self-archiving of the accepted manuscript version of this article is solely governed by the terms of such publishing agreement and applicable law.